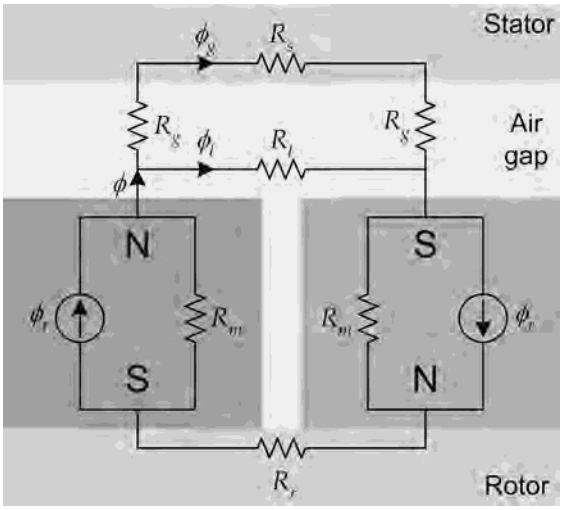

Figure 4-2. A magnetic circuit model for the structure shown in Fig. 4-1.

that travels the primary flux path across the air gap relative to the magnet flux can be estimated. That is, the air gap flux can be written in terms of the magnet flux as $\phi_g = K_l\phi$, where K_l is a leakage factor that is typically slightly less than one. Using this relationship, the next step in simplifying the magnetic circuit is to eliminate the leakage reluctance R_l as shown in Fig. 4-3*b*. Doing so is possible and desirable since very little flux follows the leakage path and since it is difficult to find an expression for R_l. To compensate for the flux that follows this leakage path, the solution for ϕ will be multiplied by an estimate of K_l to obtain ϕ_g. With the leakage reluctance eliminated, the rotor and stator ferromagnetic reluctances are in series, thereby allowing them to be lumped into a single reluctance as shown in Fig. 4-3*b* as well.

The two magnet halves in series in Fig. 4-3*b* can be combined as shown in Fig. 4-3*c*. From an electrical circuit point of view, the simplified magnetic circuit shown in Fig. 4-3*c* is found by determining the Norton equivalent circuit of the two series magnet halves. The simplified flux source is ϕ_r since that is the flux that would flow if a "short" were placed across the series magnets, and $2R_m$ is the equivalent reluctance seen looking into the circuit formed by the two series magnets. From a magnetic material point of view, the two half magnets in series is equivalent to a single block of permanent magnet material having twice the length. Therefore, the magnet flux ϕ_r remains unchanged but R_m doubles since reluctance is directly proportional to material length.

The ferromagnetic reluctance $R_r + R_s$ in Fig. 4-3*c* is nonlinear because of the saturation characteristic of ferromagnetic materials. Therefore, this ferromagnetic reluctance must be eliminated in some way to find an analytic solution. As long as the permeability of the ferromagnetic material is high relative to air, the ferromagnetic reluctance will be small relative to the air gap reluctance R_g as demonstrated

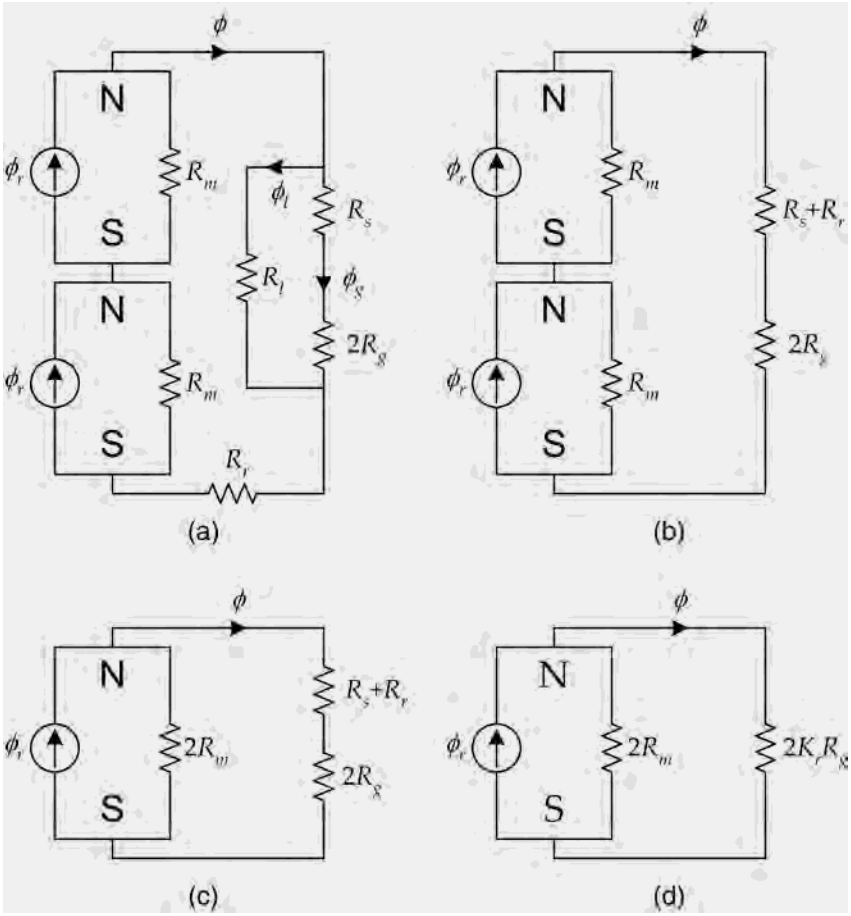

Figure 4-3. Simplifications of the magnetic circuits in Fig. 4-2.

in the example in Chapter 2. When this is true, the ferromagnetic reluctance can be thought of as a perturbation of the air gap reluctance. That is, the ferromagnetic reluctance can be eliminated by introducing a reluctance factor K_r as shown in Fig. 4-3*d*. Here K_r is a constant slightly greater than one that increases the air gap reluctance slightly to accommodate or compensate for the missing ferromagnetic reluctance.

It is important to note that in practice one seldom tries to determine analytical expressions for the leakage factor K_l and reluctance factor K_r. It is simply too difficult to determine accurate values given the simple modeling being performed here. Their values are usually chosen based on the experience of the designer.

Magnetic Circuit Solution

Given the magnetic circuit in Fig. 4-3*d*, the magnet flux ϕ can be expressed using flux division as (*i.e.*, just as one would use current division between resistors in an electrical circuit)

$$\phi = \frac{2R_m}{2R_m + 2K_r R_g}\phi_r = \frac{1}{1 + K_r \dfrac{R_g}{R_m}}\phi_r \tag{4.1}$$

Using $\phi_g = K_l \phi$ and general expressions for the magnet and air gap reluctances, *i.e.*,

$$R_m = \frac{l_m}{\mu_R \mu_o A_m}, \quad R_g = \frac{g}{\mu_o A_g} \tag{4.2}$$

the air gap flux can be written as

$$\phi_g = K_l \phi = \frac{K_l}{1 + K_r \dfrac{\mu_R g A_m}{l_m A_g}}\phi_r \tag{4.3}$$

where l_m and A_m are the magnet length and cross-sectional area respectively, and g and A_g are the air gap length and cross-sectional area respectively. Substituting the flux concentration factor $C_\phi = A_m/A_g$ from (2.30), the flux density relationships $B_g = \phi_g/A_g$ and $B_r = \phi_r/A_m$, and the permeance coefficient from (2.33) as $P_c = l_m/(g C_\phi)$ into (4.3) gives an air gap flux density of

$$B_g = \frac{K_l C_\phi}{1 + K_r \dfrac{\mu_R}{P_c}}B_r \tag{4.4}$$

This equation describes the air gap flux density crossing the air gap. For the motor being considered here with surface magnets, the leakage factor is typically in the range $0.9 \le K_l \le 1.0$, the reluctance factor is in the range $1.0 \le K_r \le 1.2$, and the flux concentration factor is ideally 1.0. If one considers these values to be fixed and the remanence B_r to be fixed by the magnet choice, the permeance coefficient P_c determines the amplitude of the air gap flux density. As the permeance coefficient increases, the air gap flux density approaches a maximum that is slightly less than the remanence. Without flux concentration, it is not possible to achieve an air gap flux density B_g greater than B_r. Moreover, the relationship between permeance coefficient and air gap flux density is nonlinear. The air gap flux density approaches the remanence asymptotically. Doubling P_c does not double B_g. However, doubling P_c means doubling the magnet length, which doubles its volume and associated cost. For typical parameter values, **Fig. 4-4** demonstrates the rela-

tionship between permeance coefficient and the ratio B_g/B_r, where the vertical lines mark the typical four to six permeance coefficient range used in many motor designs.

The flux density in (4.4) defines an approximation to the air gap flux density over the surface of the magnet pole. That is, (4.4) gives the amplitude or magnitude of the air gap flux density $|B_g|$ as shown in **Fig. 4-5**. Over North poles, (4.4) gives the positive amplitude, and over South poles, (4.4) gives the negative amplitude. While this approximation is far from exact, the derivation of (4.4) provides valuable insight into motor operation, and (4.4) itself illustrates fundamental principles that exist even when more accurate modeling is performed.

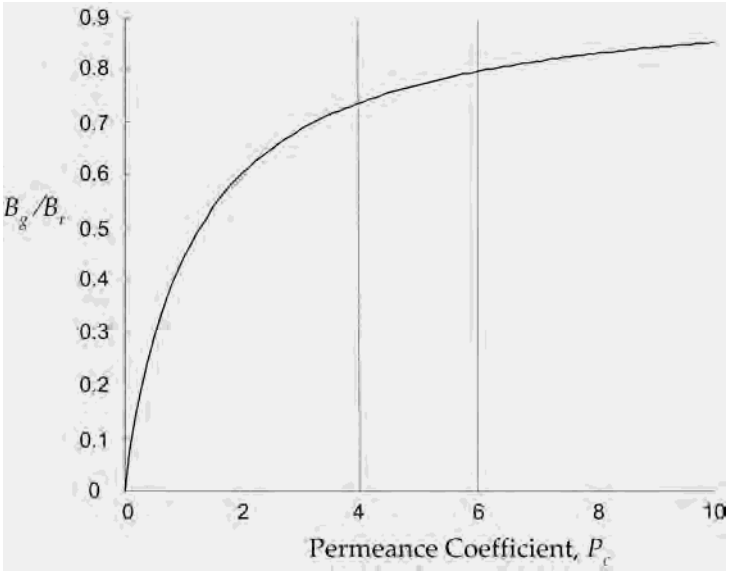

Figure 4-4. Relationship between normalized air gap flux density and permeance coefficient.

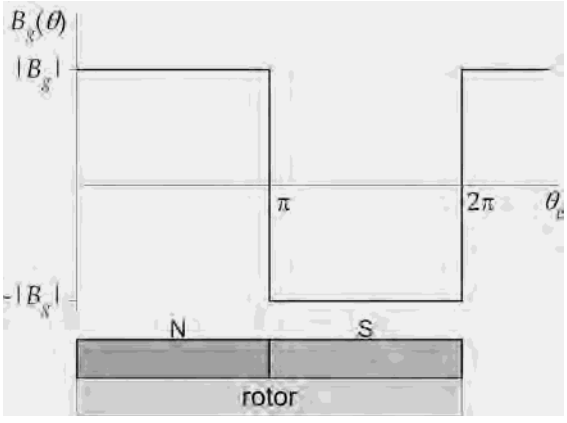

Figure 4-5. Ideal air gap flux density distribution.

For convenience, the horizontal axis in Fig. 4-5 is described in of terms electrical measure, which is periodic with respect to one pair of poles as shown in the figure. For the prototype motor being considered here, there are two electrical periods around the circumference of the rotor.

Flux Linkage

Given the solution of the magnetic circuit, consider the addition of two slots containing a winding composed of N turns of wire as shown in **Fig. 4-6**. The winding forms a coil that comes out of the slot at the top of the figure and goes into the slot on the right. The coil pitch or coil throw is 180 °E or $\theta_p = 2\pi/N_m$ radM, and the coil is said to be a full pitch winding. As the rotor turns, the air gap flux links this coil. For the rotor position shown in Fig. 4-6, the flux flows toward the South pole of the rotor magnet across the air gap from the coil. This flux flow direction is the opposite of that produced by current flowing in the coil, so the flux linkage is negative. If ϕ_g is the air gap flux as given in (4.3), the flux linkage at this position, designated $\theta_e = 0$, is $\lambda = -N\phi_g$.

If the rotor turns 90 °E as shown in **Fig. 4-7**, the coil is centered over one half of a South pole and one half of a North pole. Over the South pole the flux flows toward the rotor, while over the North pole the flux flows away from the rotor. The net flux linked by the coil is the sum of these two components, which is zero.

Rotating the rotor another 90 °E to a position $\theta_e = 180$ °E, as shown in **Fig. 4-8**, the coil is now centered over a North pole. The flux linked at this position is equal in magnitude to the flux linked at the $\theta_e = 0$ position shown in Fig. 4-6, but the direction is opposite. Therefore, the flux linkage is positive.

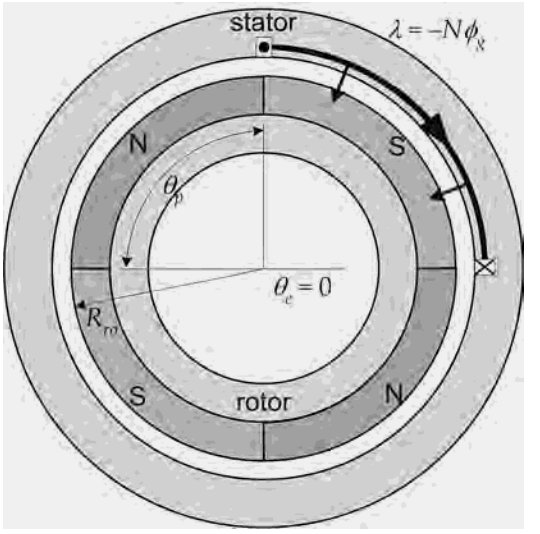

Figure 4-6. Motor having one full-pitch coil.

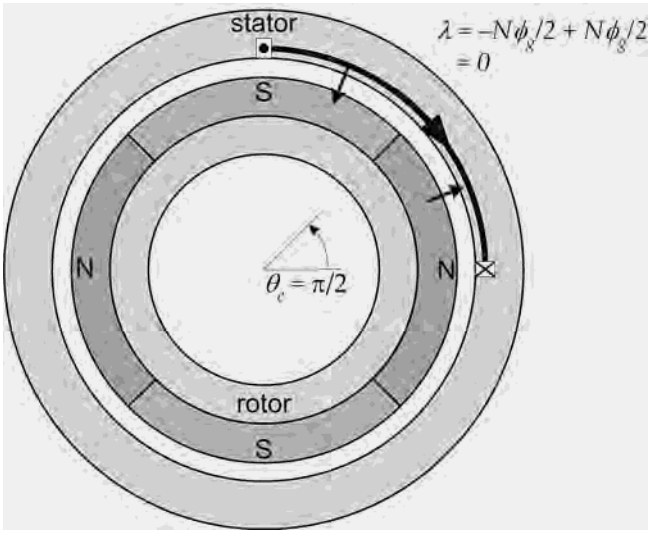

Figure 4-7. Motor with rotor at 90 °E.

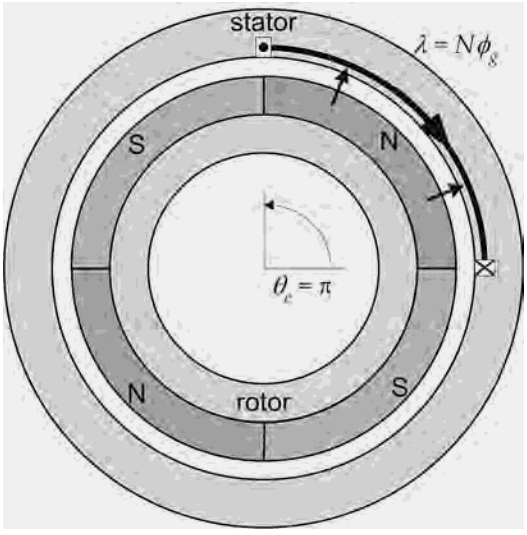

Figure 4-8. Motor with rotor at 180 °E.

At intermediate points between 0 °E and 180 °E the flux linkage varies linearly between the minimum at 0 °E and the maximum at 180 °E. Likewise, as the rotor rotates past 180 °E toward 360 °E, the flux linkage falls linearly from the maximum at 180 °E back toward another minimum at 360 °E. Further rotor rotation creates a periodic flux linkage waveform as South and North poles alternately link the coil as shown in **Fig. 4-9***a*.

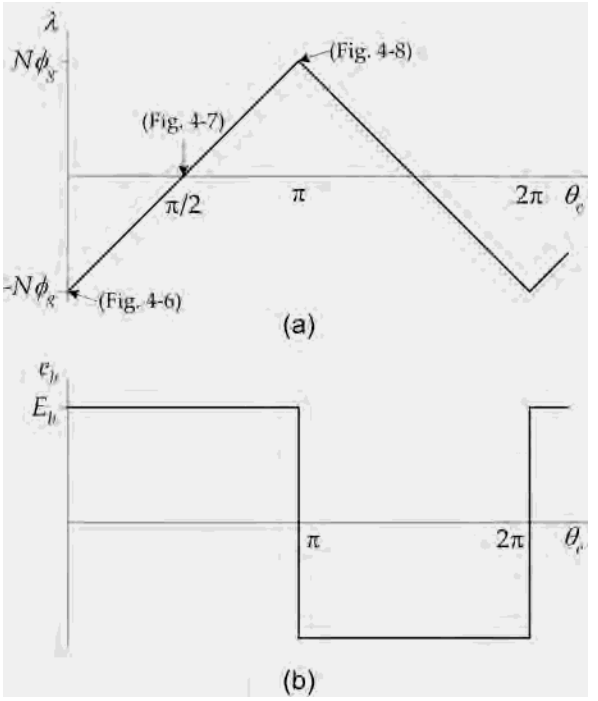

Figure 4-9. Flux linkage (a) and back EMF (b) as a function of rotor position.

Back EMF and Torque

From the flux linkage waveform shown in Fig. 4-9*a*, the associated back EMF is the derivative of the waveform as dictated by Faraday's law. Since the flux linkage is triangular in shape, the back EMF has a squarewave shape as shown in Fig. 4-9*b*. The period of the back EMF is 360 °E, thereby justifying the definition of electrical measure in Chapter 1. Analytically, the back EMF is given by

$$e_b = \frac{d\lambda}{dt} = \frac{d\theta_e}{dt}\frac{d\lambda}{d\theta_e} = \omega_e \frac{d\lambda}{d\theta_e} = \frac{N_m}{2}\omega_m \frac{d\lambda}{d\theta_e} = \frac{N_m}{2}\omega_m \frac{2N\phi_g}{\pi} \tag{4.5}$$

where ω_m is the rotor speed in radM/s. To simplify this further, the air gap flux can be written as

$$\phi_g = B_g A_g = B_g R_{ro} \theta_p L_{st} = \frac{2\pi}{N_m} B_g L_{st} R_{ro} \tag{4.6}$$

where B_g is the air gap flux density (4.4) as modified by Carter's coefficient (2.13) or (2.14) to take into account the slotting, θ_p is the angular pole pitch in radM, R_{ro} is the air gap radius at the magnet surface, and L_{st} is the axial length of the motor. Substituting this relationship into (4.5) yields the amplitude of the back EMF E_b

$$|e_b| = E_b = \frac{N_m}{2}\omega_m \frac{2N}{\pi}\left(\frac{2\pi}{N_m} B_g L_{st} R_{ro}\right) = \left(2N B_g L_{st} R_{ro}\right)\omega_m = K_e \omega_m \tag{4.7}$$

This expression agrees with the *BLv* law. The factor 2*N* is due to the two slots each having *N* conductors, and $R_{ro}\omega_m$ is the linear velocity at which the flux linkage changes. As shown on the right in (4.7), all terms in this expression except for ω_m form a back EMF constant K_e, whose units are V/(radM/s).

Application of (3.43) to (4.5) and (4.7) determines the torque produced by a current *i* flowing in the coil. Because (3.43) is a simple algebraic relationship, for constant current the torque versus position shape is the same as that for the back EMF versus position as shown in Fig. 4-9*b*. The amplitude of the torque is given by

$$|T| = \frac{E_b i}{\omega_m} = \left(2N B_g L_{st} R_{ro}\right) i = K_t i \tag{4.8}$$

All terms in (4.8) except for R_{ro} represent the force experienced by the rotor. This force acting at the radius R_{ro} gives the torque according to (1.1). From a different point of view, all terms in (4.8) except for *i* form a torque constant K_t, whose units are N·m/A. By comparing this torque constant to the back EMF constant described earlier in (4.7), they are seen to be the same quantity, *i.e.*,

$$K_e = K_t = 2N B_g L_{st} R_{ro} \tag{4.9}$$

and they are numerically equal provided the units of all terms are interpreted consistently, as they are in SI units.

The flux, flux linkage, back EMF, and torque described in this section represent an ideal situation. In reality, the air gap flux density does not have a squarewave shape as shown in Fig. 4-5. As a result, the flux linkage does not exhibit the ideal triangular shape shown in Fig. 4-9*a*, and so the back EMF is not a squarewave as shown in Fig. 4-9*b*. Much more rigor is required to accurately determine these waveforms. At the same time, the preceding analysis provides significant insight into motor operation.

Two more common and more realistic sets of waveforms are shown in **Fig. 4-10**. Because of flux leaking from magnet to magnet, motors having full pitch windings like those considered in this chapter typically exhibit a more trapezoidal back EMF waveform as shown by the lighter curves in the figure. Other motors are designed so that the flux linkage, back EMF, and torque are sinusoidal, which are shown by the darker curves in the figure. These motors typically do not have full pitch windings.

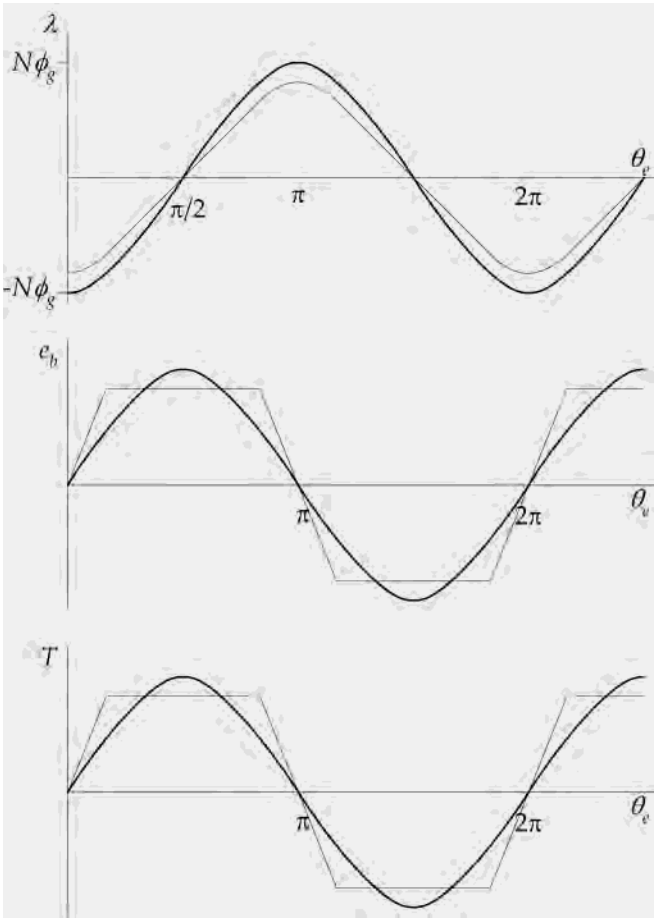

Figure 4-10. More typical flux linkage, back EMF, and torque waveforms.

Multiple Coils

The motor shown in Figs. 4-6 through 4-8 is not very efficient because room exists for more coils. The flux from three magnet poles goes unused at all times. To increase the motor performance, three more full pitch coils can be added as shown in **Fig. 4-11**. In this figure, two more slots are added, making room for the new three coils. Now each slot contains two coil sides rather than one. The first coil remains unchanged. Starting with the first coil and moving counterclockwise around the stator, each successive coil is wound in the opposite direction as the previous one. Hence, the polarity of the flux linked to each coil is the same as the preceding coil because the North and South magnet poles alternate as well.

Given the individual coils, there is flexibility about how they are connected. They may be connected in series, parallel, or a combination of series and parallel. In all cases, the collection of connected coils is called a phase winding or simply a phase.

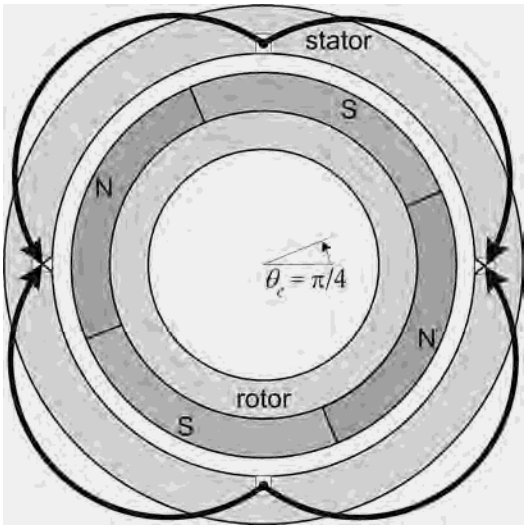

Figure 4-11. A motor having four full-pitch coils.

In many cases, all coils in a phase are connected in series. That is, the end of one coil is connected to the start of the next coil. When connected in series, the back EMFs of each coil add to become the net back EMF for the entire winding. Since the back EMF for each coil has an identical shape, the back EMF amplitude (4.7) simply changes to

$$E_b = 2 N_m N B_g L_{st} R_{ro} \omega_m \tag{4.10}$$

where $N_m = 4$ in this example. Similarly, the amplitude of the torque scales by N_m,

$$T = 2 N_m N B_g L_{st} R_{ro} i \tag{4.11}$$

This expression confirms the torque sizing relationship $T = kD^2L$ as given by (1.10). One diameter D appears as the radius R_{ro}; the other is implied by the number of magnet poles N_m, and L appears directly as L_{st}.

4.3 Multiple Phases

The motor considered in the preceding section and shown in Fig. 4-11 is a single phase motor. This motor type does not appear in many applications because it is not possible to produce torque at all rotor positions. Once every 180 °E the back EMF and torque cross through zero. At these points, the motor cannot produce torque. Moreover, if the motor comes to rest at these points, the motor cannot be started without physically rotating the shaft to a nonzero torque point.

To eliminate this problem and to make it easier to produce constant torque, brushless permanent magnet motors contain more than one phase winding, with the individual phase windings oriented so that their back EMF and torque zero

crossing points are uniformly distributed over an electrical period. Most brushless permanent magnet motors have three phases, and some have either one or two phases. Because the number of power electronics devices needed to drive a motor increases with the number of phases, it is very uncommon to see a motor having more than three phases. Only at very high power levels where multiple banks of power electronic devices are required, does it usually make sense to use more than three phases.

The motor shown in Fig. 4-11 can accommodate two additional phase windings, each composed of four coils in the same way that the first phase winding has four coils. The resulting three phase motor is shown in **Fig. 4-12**, where A, B, and C designate the phases. To avoid making the figure visually confusing, Fig. 4-12 shows only one coil for each phase. The rest are identified by the phase labels near each slot.

The phase A winding shown in Fig. 4-12 matches the phase winding described earlier in Fig. 4-11. Since there are three phases, the zero crossings of the back EMF and torque are separated by (360 °E)/3, which is 120 °E or 60 °M. Therefore the slots for phase B are rotated 60 °M from the corresponding slots of phase A, and the slots of phase C are rotated 60 °M from the corresponding slots of phase B. This arrangement places slots around the circumference of the stator every 30 °M as shown in the figure. The resulting phase waveforms are shown in **Fig. 4-13**. Since the rotor is unchanged, the flux linkage, back EMF, and torque of phase B will have the same shape as corresponding phase A waveforms, but will be delayed by the 120 °E offset due to the 120 °E offset in physical slot placement. Likewise phase C waveforms look like phase A waveforms displaced by 240 °E.

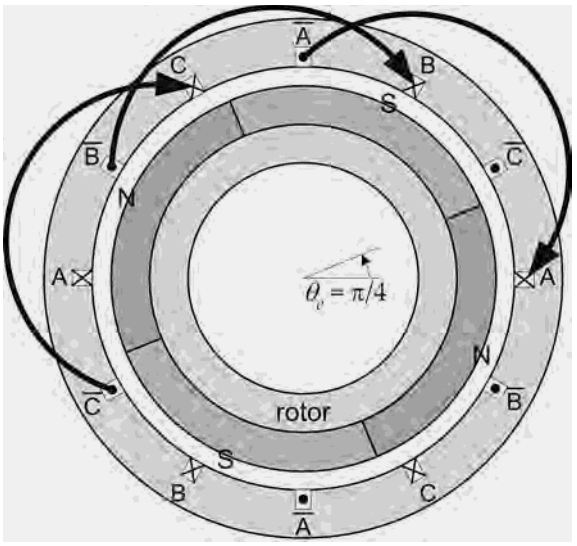

Figure 4-12. A three phase motor.

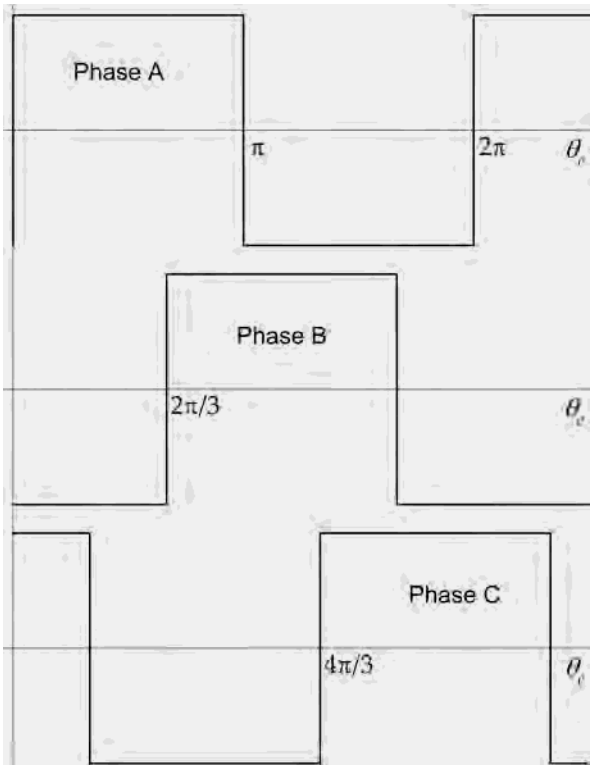

Figure 4-13. Back EMF and torque waveforms for a three phase motor.

4.4 Design Variations

The motor considered in the preceding section had full pitch coils as well as magnet poles that spanned 180 °E. In addition, all four coils in each phase were aligned with each other. That is, the back EMFs of each coil of a given phase were in phase alignment with one another. As a result, when the coils were connected in series, the net back EMF had the same shape as that for a single coil but had an amplitude four times larger. While these properties make the motor relatively easy to analyze, relatively few real motors are constructed with these properties. In this section, variations in these parameters are studied.

Fractional Pitch Coils

When the coil pitch differs from 180 °E, the winding is called a fractional pitch winding. To see how a fractional pitch winding influences the back EMF and torque, consider the motor shown in **Fig. 4-14**. Here the rotor remains unchanged, but the coil spans an angle of $\theta_c = 120$ °E, called the angular coil pitch, where the coil pitch factor is defined as $\alpha_c = \theta_c/\theta_p$. At the initial position $\theta_e = 0$ shown in the figure, the flux linkage is smaller in amplitude than the full pitch case by the coil pitch factor.